SCIENCE CHINA Information Sciences



RESEARCH PAPER

March 2026, Vol. 69, Iss. 3, 132201:1–132201:14 https://doi.org/10.1007/s11432-024-4547-5

Robust composite adaptive predefined-time control of n-link robotic systems with prescribed performance

Xiangduan ZENG¹, Changchun HUA² & Kuo LI^{2*}

¹School of Mechanical Engineering, Shijiazhuang Tiedao University, Shijiazhuang 050043, China ²School of Electrical Engineering, Yanshan University, Qinhuangdao 066004, China

Received 1 November 2024/Revised 14 May 2025/Accepted 24 July 2025/Published online 24 October 2025

Abstract This study investigates a predefined-time control approach for a class of n-link robotic systems with unknown nonlinearities. First, a time-varying scaling transformation is designed to drive the tracking errors into an adjustable range within a predefined time. Then, a novel nonsingular fast predefined-time sliding mode surface is used to develop a predefined-time controller. By introducing a simple variable-exponent coefficient in the sliding variable, the control method can achieve the prescribed performance without encountering singularities. Specifically, both transient and steady-state performances are ensured under a weaker excitation condition known as interval excitation, thereby relaxing the system's excitation requirements. Building on this, a new predefined-time parameter composite learning law is constructed by fully leveraging the information from parameter estimation errors and system tracking errors. Coupled with the predefined-time strategy, the concise relationship between the tuning gains and the predefined stabilization time is established. Theoretical analysis and experimental results confirm the proposed controller's superior performance in parameter estimation and trajectory tracking.

Keywords adaptive control, predefined-time control, prescribed performance control, composite learning, robotic systems

Citation Zeng X D, Hua C C, Li K. Robust composite adaptive predefined-time control of n-link robotic systems with prescribed performance. Sci China Inf Sci, 2026, 69(3): 132201, https://doi.org/10.1007/s11432-024-4547-5

1 Introduction

In recent years, robotic systems have played an increasingly important role in industrial production, including tasks such as assembling, assisting, transporting, drilling, and deburring [1, 2]. Due to the complexity and variability of these tasks, robotic control faces increasingly stringent requirements [3–5]. First, enabling rapid and precise estimation of complex nonlinearities under system uncertainties is essential. In addition, enhancing the transient and steady-state performance is essential. To achieve high-performance robotic control, these challenges demand further investigation.

Adaptive robust control (ARC) is well suited for robotic systems, given their uncertain and time-varying parameters [6,7]. In classical ARC, parameter update laws are systematically designed to eliminate cross terms in the Lyapunov stability analysis. However, this approach restricts parameter identification, as it relies solely on instantaneous tracking errors [8]. Due to the presence of damping terms, these methods ensure only that parameter estimates remain close to predefined values, rather than converging to the true values. Consequently, the control variable error converges to a bounded set instead of zero. To overcome these limitations, composite adaptive control (CAC) methods have been proposed [9–11]. Although CAC ensures closed-loop stability, it guarantees accurate parameter identification only when the restrictive persistent excitation (PE) condition is satisfied. This limitation has led to the recent development of composite learning control (CLC), which replaces the restrictive PE condition with the more practical interval excitation (IE) condition. Unlike CAC, which relies solely on instantaneous data, CLC also utilizes parametric information from historical data. Consequently, various advanced parameter-identification methods have been developed based on CLC [12–17]. A persistent challenge with CLC schemes is that they achieve only exponential convergence under IE conditions. To accelerate convergence, we recently proposed CL finite-time control (CLFTC) and global CL fixed-time control (GCLFTC) [18, 19]. Notably, FTC outperforms finite-time control in handling arbitrary initial conditions. However, its convergence time still lacks a direct relationship with tunable gains. This shortcoming has prompted the exploration of predefined-time stability [20-22]. To the best

^{*}Corresponding author (email: kli@ysu.edu.cn)

of our knowledge, no existing solution simultaneously guarantees: (1) predefined-time convergence of parameter estimation and tracking errors to zero, (2) singularity avoidance, and (3) operation under weak IE conditions in robotic systems.

Existing studies on adaptive robot control primarily focus on steady-state parameter convergence, with little attention to convergence rates. A key limitation of FTC, fixed-time control, and predefined-time control (PTC) methods is their insufficient consideration of transient performance indicators such as overshoot and convergence speed. In practice, controllers must meet transient performance requirements, including limits on overshoot, steady-state error, and convergence rate [23]. Therefore, simultaneously reducing overshoot and improving error convergence remain pressing challenges in robotic systems. Bechlioulis and Rovithakis introduced the widely adopted prescribed performance control (PPC) method to ensure bounded transient and steady-state errors in uncertain nonlinear systems [24]. For instance, Refs. [25, 26] employed prescribed performance functions (PPFs) combined with coordinated suspension-error transformations to regulate both transient and steady-state responses. Similarly, Refs. [27, 28] applied PPFs to enforce attitude-tracking-error bounds in spacecraft missions. However, achieving prescribed performance under weak IE conditions remains an open issue.

Herein, we focus on designing a predefined-time CL algorithm for robotic systems to achieve prescribed transient and steady-state performance bounds for position tracking errors, while ensuring the boundedness of all closed-loop signals. The main contributions of this study are summarized as follows.

- (1) In contrast to the nondifferentiable finite-time [29] and fixed-time [30] sliding variables, we develop a novel nonsingular finite-time predefined-time sliding mode (NFPTSM) by incorporating a simplified variable exponent coefficient into the sliding mode variable. Based on this innovation, a novel nonsingular CLPTC (NCLPTC) strategy is proposed. The proposed nonsingular sliding mode, independent of switching, enhances the practicality of the controller.
- (2) Unlike the restrictive PE condition, this study proposes a much weaker IE condition, which relaxes the dependence on system initial states. Different from [31,32], we construct a novel predefined-time parameter learning law that fully exploits parameter estimation errors and system tracking errors. This learning law significantly accelerates the parameter convergence rate.
- (3) Compared with [33, 34], the proposed control strategy integrates a novel coordinate transformation into the predefined-time design, allowing direct handling of time-varying asymmetric tracking error constraints. This approach eliminates the need for stringent conditions on constraint functions while preserving the original control structure. Consequently, transient and steady-state performances are guaranteed within a predefined time.

The remainder of this paper is organized as follows. Section 2 presents the background and problem formulation. Section 3 presents the development of NCLPTC. Section 4 presents the experimental results. Section 5 concludes the study.

2 Background and problem formulation

The dynamics of n-link robots are described by the Euler-Lagrange equation, as follows:

$$H(q)\ddot{q} + D(q,\dot{q})\dot{q} + F\dot{q} + g(q) = \tau, \tag{1}$$

where $q \in R^{n \times 1}$ is the vector of joint displacements, $H(q) \in R^{n \times n}$ represents the inertia matrix, $D(q, \dot{q}) \in R^{n \times n}$ represents the Coriolis and centrifugal forces, $g(q) \in R^{n \times 1}$ denotes the gravitational force, $\tau \in R^{n \times 1}$ represents the joint torque control, and $F\dot{q} \in R^{n \times 1}$ represents the viscous friction torque.

Further, the robot system exhibits the following three properties [35].

Property 1. The matrix H(q) is symmetric and positive, and there exist positive constants m_1 and m_2 satisfying $m_1 I \leq H(q) \leq m_2 I$.

Property 2. The matrix $\dot{H}(q) - 2D(q,\dot{q})$ is skew symmetric, meaning that $x^{\mathrm{T}}(\dot{H}(q) - 2D(q,\dot{q}))x = 0$ with $x \in \mathbb{R}^{n \times 1}$.

Property 3. The dynamic model of (1) can be linear in a set of unknown physical parameter vectors $\theta \in \mathbb{R}^{m \times 1}$, as

$$H(q)\dot{\xi} + D(q,\dot{q})\xi + F\dot{q} + g(q) = W^{\mathrm{T}}(q,\dot{q},\xi,\dot{\xi})\theta, \tag{2}$$

where ξ is an auxiliary variable, $W(q, \dot{q}, \xi, \dot{\xi}) \in \mathbb{R}^{m \times n}$ is a regressor matrix.

Lemma 1 ([35]). Consider a nonlinear system

$$\dot{x} = f(t, x).$$

If there exists a constant, $T_c > 0$, such that the Lyapunov function satisfies

$$\dot{V} \leqslant -\frac{\pi}{\eta T_c} (V^{1-\eta/2} + V^{1+\eta/2}),$$

 $\lim_{t\to T_c} x(t) \to 0$. The system (1) is globally predefined-time stable. Additionally, $T_c > 0$ is a predefined-time constant and $\eta \in (0,1)$.

Lemma 2 ([36]). If $x_1, x_2, ..., x_m \in \mathbb{R}^+$, and $0 < a \le 1, b > 1$, then

$$\sum_{i=1}^{m} x_i^a \geqslant \left(\sum_{i=1}^{m} x_i\right)^a, \quad \sum_{i=1}^{m} x_i^b \geqslant m^{1-b} \left(\sum_{i=1}^{m} x_i\right)^b.$$

Definition 1 ([37]). Consider a predefined-time PPF

$$\chi_i(t) = \begin{cases} (\chi_{0i} - \chi_{\infty i}) \exp(\varpi_i(t)) + \chi_{\infty i}, & 0 \leqslant t < T_i, \\ \chi_{\infty i}, & t \geqslant T_i, \end{cases}$$
 (3)

where $\dot{\chi}_i(t) = \{(\chi_{0i} - \chi_{\infty i})\dot{\varpi}_i(t)\exp(\varpi_i(t)), \ 0 \leqslant t < T_i|0, \ t \geqslant T_i\}, \ \varpi_i(t) = -\frac{l_i T_i t}{T_i - t}, \ 0 < \chi_{\infty i} < \chi_{0i}. \ 0 < T_i < \infty,$ and $l_i > 1$. Here, T_i is the time taken for the function to converge from χ_{0i} to $\chi_{\infty i}$.

Definition 2 ([6]). A bounded signal $\Phi(t) \in \mathbb{R}^{m \times n}$ satisfies the IE condition

$$\int_{T_e - t_d}^{T_e} \Phi^{\mathrm{T}}(r)\Phi(r)\mathrm{d}r \geqslant \sigma I,\tag{4}$$

for $\exists T_e, t_d, \sigma \in \mathbb{R}^+, t \in [T_e - t_d, T_e], \sigma$ is the excitation strength.

Definition 3 ([6]). A bounded signal $\Phi(t) \in \mathbb{R}^{m \times n}$ satisfies the PE condition

$$\int_{t-t_d}^t \Phi^{\mathrm{T}}(r)\Phi(r)\mathrm{d}r \geqslant \sigma I,\tag{5}$$

for $\exists t_d, \sigma \in \mathbb{R}^+$ and $\forall t > 0, \sigma$ are the excitation strength.

Remark 1. The use of a time-varying scaling transformation to drive tracking errors within a preset range offers several advantages. First, it enables precise tracking performance by dynamically adjusting the scaling factors based on the current state of the tracking errors. This ensures that errors remain within an acceptable range, thereby enhancing the system's accuracy and reliability. Second, the time-varying nature of the scaling transformation allows the system to adapt to changes in operating conditions or external disturbances, maintaining robust performance. This adaptability is particularly valuable in dynamic environments where system behavior may vary significantly over time. Moreover, driving tracking errors into a predefined range provides better control over system output, which is beneficial for applications that demand tight regulation or strict performance criteria. Overall, the time-varying scaling transformation offers a powerful and flexible approach to achieving accurate and robust tracking in control systems.

Remark 2. Compared with the PE condition, the IE condition imposes more relaxed requirements. The PE condition demands that the system input signal remain sufficiently active over time to ensure accurate parameter identification. However, such stringent requirements can be difficult or costly to meet in practical applications. In contrast, the IE condition only requires that the input signal contain sufficient information within specific time intervals to update the system parameters, thereby reducing the continuous demand on the system input. This makes the IE condition more feasible in practice, particularly in resource-constrained or complex environments. Furthermore, although the PE condition was originally proposed to guarantee accurate parameter identification, such strictness is not always necessary. Certain learning algorithms perform better under tailored excitation conditions, making the IE condition more suitable for those cases. By relaxing excitation requirements, the IE condition supports learning performance while easing the continuous input demand, offering clear advantages in practical scenarios. This flexibility makes the IE condition a valuable excitation strategy in CL.

In this study, $q_d(t) \in \mathbb{R}^n$ is the reference signal trajectory, satisfying the condition $q_d(t), \dot{q}_d(t), \ddot{q}_d(t) \in L_{\infty}$, and $\hat{\theta}$ is employed for the estimation for θ . Based on the above definition, $e(t) = q(t) - q_d(t)$ and $\tilde{\theta} = \theta - \hat{\theta}$ were obtained.

3 Main results

3.1 Universal time-varying asymmetric-error transformation

The prescribed function, $\psi(\cdot): (\underline{d}_i, \overline{d}_i) \to (-\infty, \infty)$, is denoted as follows:

$$\psi(x) = \ln\left(\frac{\bar{d}_i(x - \underline{d}_i)}{-\underline{d}_i(\bar{d}_i - x)}\right). \tag{6}$$

Notably, Eq. (6) is strictly monotonically increasing for any scalar variable, x, where $\psi(0) = 0$, $\lim_{x \to \underline{d}_i} \psi(x) = -\infty$, and $\lim_{x \to \overline{d}_i} \psi(x) = \infty$.

Further, the inverse function of $\psi(x)$ is given by the following:

$$\psi(x)^{-1} = \frac{\underline{d}_i \overline{d}_i(\exp(x) - 1)}{\underline{d}_i \exp(x) - \overline{d}_i}.$$
 (7)

It can be inferred that $\psi(x)^{-1}_{x\to\infty}\to (\underline{d}_i,\overline{d}_i)$ and $\psi(x)^{-1}(0)=0$. Thus, the prescribed performance can be rewritten as

$$\underline{d}_i \chi_i(t) < e_i(t) < \bar{d}_i \chi_i(t), \tag{8}$$

where $\chi_i(t)$ is the PPF, the position-tracking error, $e = q - q_d$, is the desired trajectory, and \underline{d}_i and \overline{d}_i can be described, as follows:

$$\underline{d}_{i} = \begin{cases} -\vartheta_{i}, & e_{i}(0) \geqslant 0, \\ -1, & e_{i}(0) < 0, \end{cases} \quad \bar{d}_{i} = \begin{cases} \vartheta_{i}, & e_{i}(0) \geqslant 0, \\ 1, & e_{i}(0) < 0, \end{cases}$$
(9)

where $\vartheta_i \in (0,1)$ is a constant with respect to the adjustable overshoot, $e(t) = [e_1(t), \dots, e_n(t)]^T$, and $e_i(0)$ is the initial position-tracking error.

To analyze the latter content, the following auxiliary variable, ϱ_i , is designed:

$$\varrho_i = \frac{e_i}{\chi_i}.\tag{10}$$

In Eqs. (6) and (10), we introduce the ith component of ζ , as follows:

$$\zeta_i = \psi(\rho_i). \tag{11}$$

The time derivative of (11) is given, as follows:

$$\dot{\zeta}_i = \beta_i (\dot{e}_i + \alpha_i e_i), \tag{12}$$

and

$$\alpha_i = -\dot{\chi}_i/\chi_i, \quad \beta_i = \upsilon(\varrho_i)/\chi_i. \tag{13}$$

From Definition 1, as $\chi_i > 0$ and $\dot{\chi}_i \leq 0$, it follows that $\alpha_i \geq 0$. Additionally, by combining (13) with $\chi_i^{-1} \geq \chi_{0i}^{-1} > 0$, we obtain

$$\beta_i > 2\chi_{0i}^{-1}. \tag{14}$$

Thus, the vector form of (12) can be described by the following equation:

$$\dot{\zeta} = \gamma_1 \dot{e} + \gamma_2,\tag{15}$$

where $\dot{\zeta} = [\dot{\zeta}_1, \dots, \dot{\zeta}_n]^T \in \mathbb{R}^n$, $\gamma_1 = \text{diag}\{\gamma_{1i}\} \in \mathbb{R}^{n \times n}$, $\gamma_2 = [\gamma_{21}, \dots, \gamma_{2n}]^T \in \mathbb{R}^n$, $\gamma_{1i} = \beta_i, \gamma_{2i} = \beta_i \alpha_i e_i, i = 1, \dots, n$. Based on (13) and (14), we obtain $\gamma_{1i} > 0$, yielding the positive definiteness of matrix γ_1 . Moreover, γ_1 and γ_2 are readily accessible for subsequent controller designs.

Based on (15), Eq. (1) can be rewritten as

$$H(q)\gamma_1^{-1}\ddot{\zeta} + (Hd(\gamma_1^{-1})/dt + D\gamma_1^{-1})\dot{\zeta} + F\dot{q} + Hd(\dot{q}_d - \gamma_1^{-1}\gamma_2)/dt + D(\dot{q}_d - \gamma_1^{-1}\gamma_2) + g(q) = \tau.$$
 (16)

Consider (16) with γ_1^{-1} , the following can be achieved:

$$M(q,\gamma_1)\ddot{\zeta} + C(q,\dot{q},\gamma_1,\dot{\gamma}_1)\dot{\zeta} + \Im(q,\dot{q},\gamma_1,\dot{\gamma}_1,\gamma_2,\dot{\gamma}_2) = \gamma_1^{-1}\tau, \tag{17}$$

where $M = \gamma_1^{-1} H \gamma_1^{-1}$, $C = \gamma_1^{-1} H \operatorname{d}(\gamma_1^{-1}) / \operatorname{d}t + \gamma_1^{-1} D \gamma_1^{-1}$, $\Im = \gamma_1^{-1} [D(\dot{q}_d - \gamma_1^{-1} \gamma_2) + F \dot{q} + g + H \operatorname{d}(\dot{q}_d - \gamma_1^{-1} \gamma_2) / \operatorname{d}t]$. Remark 3. Properties 1–3 confirm that the system, (17), exhibits the following attributes. (1) $M(q, \gamma_1)$ and H(q) have similar properties. Both are positive definite matrices, and there exist $c_1 \in R^+$ and $c_2 \in R^+$ such that $c_1 I \leq M(q, \gamma_1) \leq c_2 I$. (2) Similarly, $x^{\mathrm{T}}(\dot{M}(q, \gamma_1) - 2C(q, \dot{q}, \gamma_1, \dot{\gamma}_1))x = 0$, $x \in R^{n \times 1}$. The matrix, $\dot{M}(q, \gamma_1) - 2C(q, \dot{q}, \gamma_1, \dot{\gamma}_1)$, is skew-symmetric. (3) The dynamical equation, (17), is linear, comprising a set of unknown physical parameter vectors θ .

$$M(q,\gamma_1)\dot{\xi} + C(q,\dot{q},\gamma_1,\dot{\gamma}_1)\xi + \Im(q,\dot{q},\gamma_1,\dot{\gamma}_1,\gamma_2,\dot{\gamma}_2) = \bar{W}^{\mathrm{T}}(q,\dot{q},\gamma_1,\dot{\gamma}_1,\gamma_2,\dot{\gamma}_2,\xi,\dot{\xi})\theta,\tag{18}$$

where $W(q, \dot{q}, \gamma_1, \dot{\gamma}_1, \gamma_2, \dot{\gamma}_2, \xi, \dot{\xi})$ is the regressor matrix. Based on the above analysis, we reformulate the dynamical equation, (1), obtaining an equivalent "unconstrained" system (17).

Remark 4. Following the quantitative formulation of the transient and steady-state performance constraints of the controlled system, we further introduced upper and lower bound constraints into the control system, thereby increasing the complexity of designing the corresponding controller. To achieve the subsequent controller design, the constrained nonlinear system must be converted into an unconstrained one. Additionally, finding an error-transformation function that enables homeomorphic mapping is key to achieving an equivalent transformation from the performance-constrained space to an unconstrained space. Compared with the original system, the transformed nonlinear system is unconstrained. Therefore, utilizing this new transformed system reduces the complexity of controller designs. As a homeomorphic mapping exists between the original and new systems, the subsequent controller design must only ensure that the states of the mapped system are bounded without relying on the constraint conditions of the original system. Notably, constraints do not necessarily change the control structure that is designed for the transformed nonlinear system. In this study, we offered a supplementary explanation.

3.2 NCLPTC design

Here, we design a novel CLPTC strategy. The objective is to achieve PTC and parameter identification without encountering singularities. Notably, this is accomplished under the lenient, weak IE condition. According to Property 3, the robotic model (1) can be writen as follows:

$$\tau = W^{\mathrm{T}}(q, \dot{q}, \ddot{q})\theta. \tag{19}$$

One may observe that the regressor matrix $W(q, \dot{q}, \ddot{q})$ includes the joint acceleration (\ddot{q}) , which is sensitive to measurement noise. To reduce reliance on acceleration information (\ddot{q}) , the following linear filter [9] is adopted:

$$\dot{\tau}_f(t) = \alpha(\tau(t) - \tau_f(t)),\tag{20}$$

$$\dot{W}_f^{\mathrm{T}}(q, \dot{q}) = \alpha (W^{\mathrm{T}}(q, \dot{q}, \ddot{q}) - W_f^{\mathrm{T}}(q, \dot{q})), \tag{21}$$

where $\tau_f(0) = 0$, $\alpha \in \mathbb{R}^+$ is a filtering constant, $\tau_f(t)$ and $W_f(q, \dot{q})$ are the filtered counterparts of $\tau(t)$ and $W(q, \dot{q}, \ddot{q})$, respectively, and the initial condition is $W_f^{\mathrm{T}}(0) = 0$. The filtered robotic model is expressed as follows:

$$\tau_f = W_f^{\mathrm{T}}(q, \dot{q})\theta. \tag{22}$$

By multiplying both sides of (22) by $W_f(q, \dot{q})$ and integrating the resulting equality over the interval $[t - t_d, t]$, we obtain

$$\Theta(t) = \int_{t-t_d}^t W_f(q(\varphi), \dot{q}(\varphi)) W_f^{\mathrm{T}}(q(\varphi), \dot{q}(\varphi)) d\varphi, \tag{23}$$

$$\Theta(t)\theta = \int_{t-t_d}^t W_f(q(\varphi), \dot{q}(\varphi)) \tau_f(\varphi) d\varphi, \tag{24}$$

where $\Theta(t)$ is called the excitation matrix. If the IE condition is satisfied, then according to Definition 1, there exist positive constants T_e , t_d , and σ such that $\Theta(T_e) \geqslant \sigma I$.

Next, a prediction error (ε) and a modified excitation matrix $(\bar{\Theta}(t))$ are defined as follows:

$$\varepsilon(t) = \begin{cases} \Theta(T_e)\theta - \Theta(T_e)\hat{\theta}, \\ \Theta(t)\theta - \Theta(t)\hat{\theta}, \end{cases} \bar{\Theta}(t) = \begin{cases} \Theta(T_e), \ t \geqslant T_e, \\ \Theta(t), \ t < T_e. \end{cases}$$
 (25)

According to (25), we immediately obtain

$$\varepsilon(t) = \bar{\Theta}(t)\tilde{\theta}. \tag{26}$$

Subsequently, the parameter composite learning law is formulated as follows:

$$\dot{\hat{\theta}} = \Gamma P \left(\bar{\Theta}^{\mathrm{T}} \frac{\pi}{2\eta T_c} \left(\left(\frac{1}{2} \varepsilon^{\mathrm{T}} \Gamma^{-1} \varepsilon \right)^{-\frac{\eta}{2}} + \left(\frac{1}{2} \varepsilon^{\mathrm{T}} \Gamma^{-1} \varepsilon \right)^{\frac{\eta}{2}} \right) \Gamma \varepsilon + \bar{W}^{\mathrm{T}} (q, \dot{q}, \gamma_1, \dot{\gamma}_1, \gamma_2, \dot{\gamma}_2, \dot{\zeta}_r, \ddot{\zeta}_r) s \right), \tag{27}$$

where $\bar{W}^{\mathrm{T}}(q,\dot{q},\gamma_{1},\dot{\gamma}_{1},\gamma_{2},\dot{\zeta}_{r},\ddot{\zeta}_{r})$ is the regressor matrix. For ease of computation, we replaced $\bar{W}^{\mathrm{T}}(q,\dot{q},\gamma_{1},\dot{\gamma}_{1},\gamma_{2},\dot{\gamma}_{2},\dot{\zeta}_{r},\ddot{\zeta}_{r})$ with \bar{W}^{T} . Notably, s is the NFPTSM, which will be discussed below. $\Gamma \in R^{m \times m}$ are the feedback gain matrices. In the preceding section, we designed PTCL. Based on this, we designed the predefined-time controller as shown in Figure 1 and discussed in the next section.

To guarantee CLPTC without encountering singularities, NFPTSM, $s = \text{col}\{s_i\}$, is constructed, as follows:

$$s_i = \dot{\zeta}_i + \frac{\omega_i}{T_{si}} k_i |\zeta_i|^{\frac{\lambda_i \zeta_i^2}{1 + \mu_i \zeta_i^2}} \operatorname{sign}(\zeta_{1i}), \tag{28}$$

where $\omega_i \geqslant (1/k_i(\theta_i - 1) + 1/k_i e^{-\frac{\lambda_i}{2e}})$, with $\zeta_i \in R$, $\lambda_i > 0$, and $\mu_i > 0$ such that $\iota_i = \frac{\lambda_i}{1 + \mu_i} > 1$.

Remark 5. This study presents a novel finding on global robust predefined-time stability using constant and state-dependent variable exponent coefficients. To the best of our knowledge, these coefficients have not been previously used in predefined-time stability analysis. By adopting the sliding mode control (SMC) method, we achieve global robust asymptotic stability for a class of uncertain robotic systems. Furthermore, robust predefined-time stability of the sliding-mode variable system is realized using constant exponential coefficients in the sliding-mode variable and the controller. By introducing state-dependent variable exponential coefficients into both components, we also achieve global robust predefined-time stability. The proposed sliding-mode controller is time-independent, nonsingular, robust to finite disturbances, and easy to implement. Compared with the constant exponent strategy, the use of variable exponential coefficients allows robust predefined-time SMC. Achieving predefined-time stability of the global system using sliding-mode control is challenging due to the singularities that may arise with the simplest sliding-mode variables. However, by simultaneously using variable exponential coefficients in both the sliding-mode variable and controller, we propose a simple solution to eliminate these singularities.

Remark 6. Note that the function, $\varphi_i: \zeta_i \to |\zeta_i|^{\frac{\lambda_i \zeta_i^2}{1+\mu_i \zeta_i^2}} = \exp(\frac{\lambda_i \zeta_{1i}^2}{1+\mu_i \zeta_i^2} \ln(|\zeta_i|))$, is continuous at $\zeta_i = 0$ with $\varphi_i(0) = 1$. Therefore, the right-hand side of (28) is locally bounded. Consider the following quadratic Lyapunov function:

$$V_i(\zeta_i) = \zeta_i^2. \tag{29}$$

The equation yields

$$\dot{V}_i(\zeta_i) = -2\frac{\omega_i}{T_{si}} k_i |\zeta_i|^{\frac{\lambda_i \zeta_i^2}{1 + \mu_i \zeta_i^2} + 1}.$$
(30)

Consider the case, $V_i(\zeta_{1i}) \geqslant 1$. We then have $\frac{\lambda_i \zeta_i^2}{1 + \mu \zeta_i^2} + 1 \geqslant \frac{\lambda_i}{1 + \mu_i} + 1 > 2$. As $|\zeta_i| \geqslant 1$ and $\iota_i = \frac{\lambda_i}{1 + \mu_i} > 1$, it exhibits

$$\dot{V}_i(\zeta_i) \leqslant -2\frac{\omega_i}{T_{ci}} k_i |\zeta_i|^{\iota_i + 1} \leqslant -2\frac{\omega_i}{T_{ci}} k_i V_i(\zeta_i)^{\frac{\iota_i + 1}{2}}.$$
(31)

Furthermore, $k_i > 0$ and $\frac{\theta_i + 1}{2} > 1$ ensure that all the solutions beginning from $V(\zeta_i) \ge 1$ reach the set, $V(\zeta_i) \le 1$, in a predefined time, $T_{1i} \le \frac{T_{ci}}{\omega_i k_i (\iota_i - 1)}$.

In case $V_i(\zeta_i) \leq 1$, we obtain

$$\dot{V}_i(\zeta_i) = -2 \frac{\omega_i}{T_{ci}} k_i |\zeta_i|^{\frac{\lambda_i \zeta_i^2}{1 + \mu_i \zeta_i^2}}, \tag{32}$$

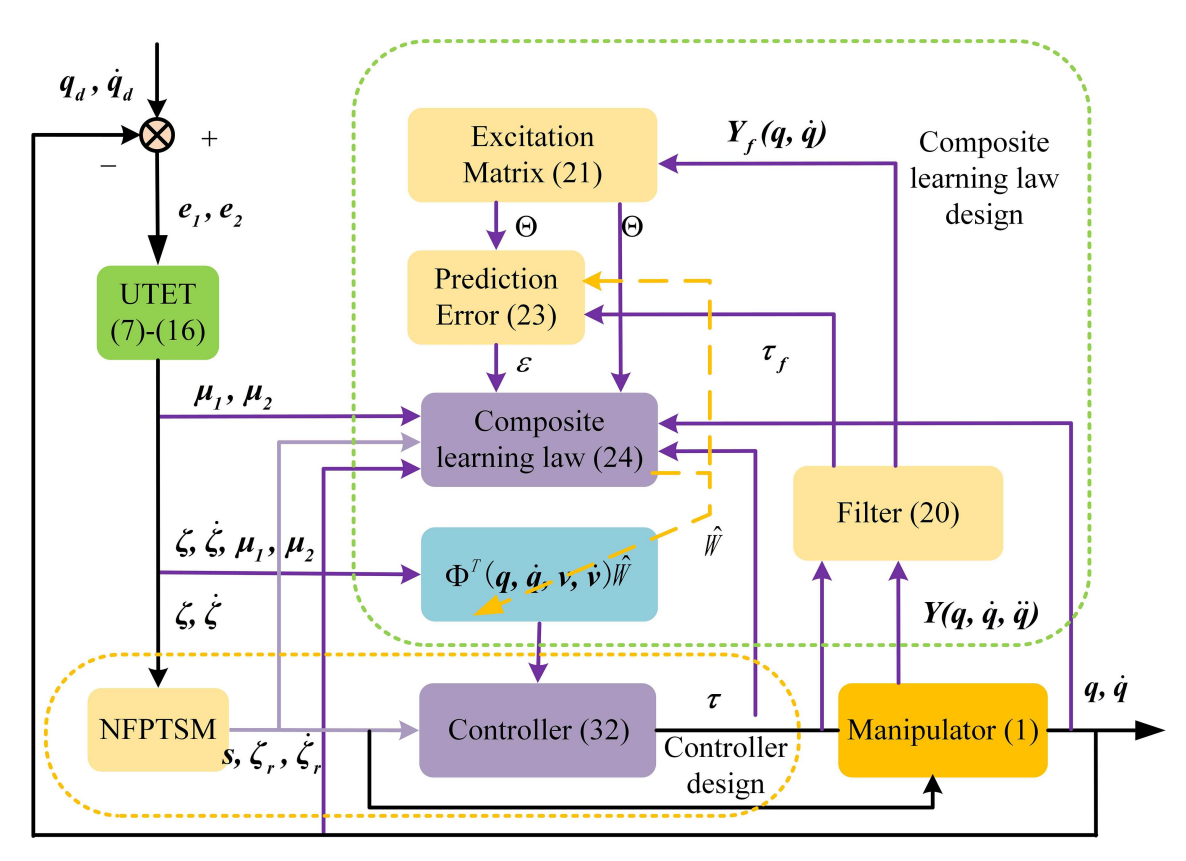


Figure 1 (Color online) Schematic of the proposed control strategy.

where $1 + \mu_i \zeta_i^2 \geqslant 1$ and $|\zeta_i| \leqslant 1$. We obtain $\min(|\zeta_i|^{\frac{\lambda_i \zeta_i^2}{1 + \mu_i \zeta_i^2}}) \geqslant \min(|\zeta_i|^{\lambda_i \zeta_{1i}^2}) = e^{\frac{-\lambda_i}{2e}}$, and subsequently

$$\dot{V}_i(\zeta_i) \leqslant -2\frac{\omega_i}{T_{ci}} k_i e^{\frac{-\lambda_i}{2e}} |\zeta_i| \leqslant -2\frac{\omega_i}{T_{ci}} k_i e^{\frac{-\lambda_i}{2e}} V_i(\zeta_i)^{\frac{1}{2}}.$$

$$(33)$$

With $k_i e^{\frac{-\lambda_i}{2e}} > 0$, all the solutions starting from $V_i(\zeta_i) \leqslant 1$ reach the origin in a uniform time $T_{2i} \leqslant \frac{T_{ci}}{\omega_i k_i e^{\frac{-\lambda_i}{2e}}}$. Finally, system (28) reaches the origin in a predefined time $T_{si}(x_0) \leqslant T_{1i} + T_{2i}$. This means that $T_{si}(x_0) \leqslant \frac{T_{ci}}{\omega_i} (\frac{1}{k_i(\theta_{i}-1)} + \frac{1}{k_i e^{-\frac{\lambda_i}{2e}}})$. Select $\omega_i \geqslant (\frac{1}{k_i(\theta_{i}-1)} + \frac{1}{k_i e^{-\frac{\lambda_i}{2e}}})$, we have $T_{si}(x_0) \leqslant T_{ci}$.

This indicates that the NFPTSM converges to the origin within the predefined time.

Based on (17), (28) and Property 6, the following can be achieved:

$$M(q, \gamma_1)\dot{s} + C(q, \dot{q}, \gamma_1, \dot{\gamma}_1)s = \gamma_1^{-1}\tau - \bar{W}^{\mathrm{T}}\theta.$$
(34)

Thus, the control law is designed as follows:

$$\tau = -\gamma_1 \left(\left(\frac{\pi}{2\eta T_c} \left(\left(\frac{1}{2} s^{\mathrm{T}} \Gamma^{-1} s \right)^{-\eta/2} + \left(\frac{1}{2} s^{\mathrm{T}} \Gamma^{-1} s \right)^{\eta/2} \right) \right) M s + \bar{W}^{\mathrm{T}} \hat{\theta} \right), \tag{35}$$

where matrices $\Gamma^{-1} \in \mathbb{R}^{n \times n}$ are positive and diagonal-definite.

Applying (34) to (35) yields the closed-loop dynamics, as follows:

$$M(q, \mu_1)\dot{s} + C(q, \dot{q}, \mu_1, \dot{\mu}_1)s = -\bar{W}^{\mathrm{T}}\tilde{\theta} - \frac{\pi}{2\eta T_c} \left(\left(\left(\frac{1}{2} s^{\mathrm{T}} \Gamma^{-1} s \right)^{-\eta/2} + \left(\frac{1}{2} s^{\mathrm{T}} \Gamma^{-1} s \right)^{\eta/2} \right) Ms \right). \tag{36}$$

3.3 Stability analysis

The following results can be obtained based on Subsection 3.2.

Theorem 1. For the robotic system, (1), with the parameter-learning law, (27), and the controller, (35), there exists $T_e > 0$, which satisfies the IE condition, $\Theta(T_e) \geqslant \sigma I$, $\sigma, t_d \in R^+$. Based on this, we obtained the following. (1) e_i is always stable in $(\underline{d}_i\chi_i, \overline{d}_i\chi_i)$ and converges to $(\underline{d}_i\chi_{\infty i}, \overline{d}_i\chi_{\infty i})$ at T_i . (2) $\tilde{\theta}$ and e converge to zero within a predefined time, T_f , during which $T_f \leqslant T_s + T_c + T_e$, $T_s = \max\{T_{s1}, \ldots, T_{sn}\}$. Further, $T_c = \max\{T_{c1}, \ldots, T_{cn}\}$ are known positive constants.

Proof. First, consider the Lyapunov candidate function V_1 :

$$V_1 = \frac{1}{2} s^{\mathrm{T}} M(q, \gamma_1) s. \tag{37}$$

By differentiating V_1 and using (34), one achieves

$$\dot{V}_1 = s^{\mathrm{T}} \left(\gamma_1^{\mathrm{T}} \tau - \bar{W}^{\mathrm{T}} \theta + \frac{1}{2} \dot{M} s - D s \right). \tag{38}$$

Based on Properties 4 and 5, we obtained

$$\dot{V}_1 = s^{\mathrm{T}} (\gamma_1^{\mathrm{T}} \tau - \bar{W}^{\mathrm{T}} \theta). \tag{39}$$

Substituting the control law, (35), into (39) yields

$$\dot{V}_1 = s^{\mathrm{T}} \bar{Y}^{\mathrm{T}} \tilde{\theta} - \frac{\pi}{2\eta T_c} s^{\mathrm{T}} \pi M s, \tag{40}$$

where $\pi = (\frac{1}{2}s^{\mathrm{T}}\Gamma^{-1}s)^{-\frac{\eta}{2}} + (\frac{1}{2}s^{\mathrm{T}}\Gamma^{-1}s)^{\frac{\eta}{2}}$.

Second, considering the Lyapunov candidate function V_2 :

$$V_2 = \frac{1}{2} s^{\mathrm{T}} M(q, \gamma_1) s + \frac{1}{2} \tilde{\theta}^{\mathrm{T}} \Gamma^{-1} \tilde{\theta}.$$

$$\tag{41}$$

The derivative of V_2 can be obtained as

$$\dot{V}_2 = -s^{\mathrm{T}} \frac{\pi}{2\eta T_c} \pi M s + \tilde{\theta} (s^{\mathrm{T}} W - \Gamma^{-1} \dot{\hat{\theta}}). \tag{42}$$

Relying on the characteristics of the projection operation in [38], the parameter update law guarantees $\hat{\theta}(t) \in \Omega_{c_{\theta}}$ with $\hat{\theta}(0) \in \Omega_{c_{\theta}}$ and $\tilde{\theta}(s^{\mathrm{T}}Y - \Gamma^{-1}\dot{\hat{\theta}}) \leqslant -\tilde{\theta}\bar{\Theta}^{\mathrm{T}}\frac{\pi}{2\eta T_{c}}((\frac{1}{2}\varepsilon^{\mathrm{T}}\Gamma^{-1}\varepsilon)^{-\eta/2} + (\frac{1}{2}\varepsilon^{\mathrm{T}}\Gamma^{-1}\varepsilon)^{\eta/2})\Gamma^{-1}\varepsilon$. Employing the predefined-time CL update law (27), and Eq. (26) yields

$$\dot{V}_{2} \leqslant -\frac{\pi}{2\eta T_{c}} \left(\left(\frac{1}{2} s^{\mathrm{T}} M s \right)^{1-\eta/2} + \left(\frac{1}{2} s^{\mathrm{T}} M s \right)^{1+\eta/2} \right)
-\frac{\pi}{2\eta T_{c}} \left(\left(\frac{1}{2} \varepsilon^{\mathrm{T}} \Gamma^{-1} \varepsilon \right)^{1-\eta/2} + \left(\frac{1}{2} \varepsilon^{\mathrm{T}} \Gamma^{-1} \varepsilon \right)^{1+\eta/2} \right).$$
(43)

As the IE condition holds that $\Theta(t) \geq \sigma I$, we obtained

$$\dot{V}_{2} \leqslant -\frac{\pi}{2\eta T_{c}} \left(\left(\frac{1}{2} s^{\mathrm{T}} M s \right)^{\frac{1-\eta}{2}} + \sigma^{2-\eta} \left(\frac{1}{2} \tilde{\theta}^{\mathrm{T}} \Gamma^{-1} \tilde{\theta} \right)^{\frac{1-\eta}{2}} \right)
-\frac{\pi}{2\eta T_{c}} \left(\left(\frac{1}{2} s^{\mathrm{T}} M s \right)^{\frac{1+\eta}{2}} + \sigma^{2+\eta} \left(\frac{1}{2} \tilde{\theta}^{\mathrm{T}} \Gamma^{-1} \tilde{\theta} \right)^{\frac{1+\eta}{2}} \right).$$
(44)

Further, by defining $k_1 = \min\{1, \sigma^{2-\eta}\}$ and $k_2 = \min\{1, \sigma^{2+\eta}\}$, and according to Lemma 2, we obtained the following:

$$\dot{V}_{2} \leqslant -\frac{\pi}{2\eta T_{c}} k_{1} \left(\left(\frac{1}{2} s^{\mathrm{T}} M s + \frac{1}{2} \tilde{\theta}^{\mathrm{T}} \Gamma^{-1} \tilde{\theta} \right)^{1-\eta/2} \right)
-\frac{\pi}{2\eta T_{c}} k_{2} \left(\left(\frac{1}{2} s^{\mathrm{T}} M s + \frac{1}{2} \tilde{\theta}^{\mathrm{T}} \Gamma^{-1} \tilde{\theta} \right)^{1+\eta/2} \right).$$
(45)

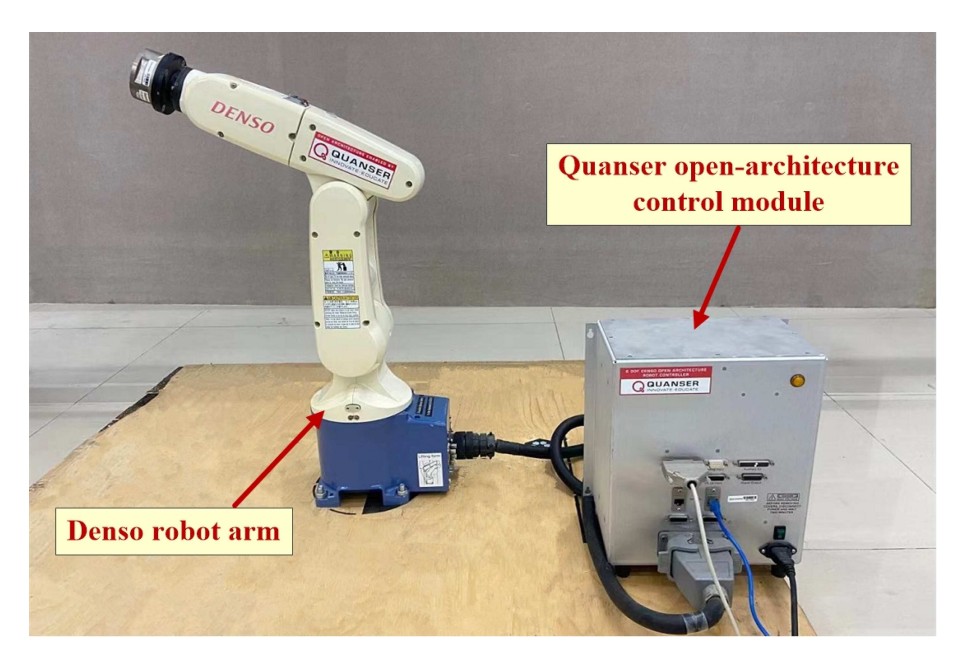


Figure 2 (Color online) Illustration of the experimental platform.

Employing (41) and (45) yields

$$\dot{V}_2 \leqslant -\frac{\pi}{2\eta T_c} k \left(V_2^{1-\eta/2} + V_2^{1+\eta/2} \right),$$
 (46)

where $k = \min\{k_1, k_2\}.$

Based on (46) with Lemma 1, we confirmed that the sliding-mode surface, s, converged to zero in a predefined time. Based on (10) and (11), we deduced the following:

$$e_i = \chi_i \psi^{-1}(\zeta_i). \tag{47}$$

Based on Lemma 3, the information presented in (7) regarding $\psi^{-1}(0) = 0$ and the bounded positivity of χ_i confirmed that e_i and ζ_i globally converged to zero in a predefined time.

The preceding analysis revealed that $\zeta_i \in L_{\infty}$ holds for $t \geq 0$. Consequently, by integrating $\psi^{-1}(\zeta_i) \in (\underline{\chi}_i, \overline{\chi}_i)$ from (7), we characterized the range of (47), as follows:

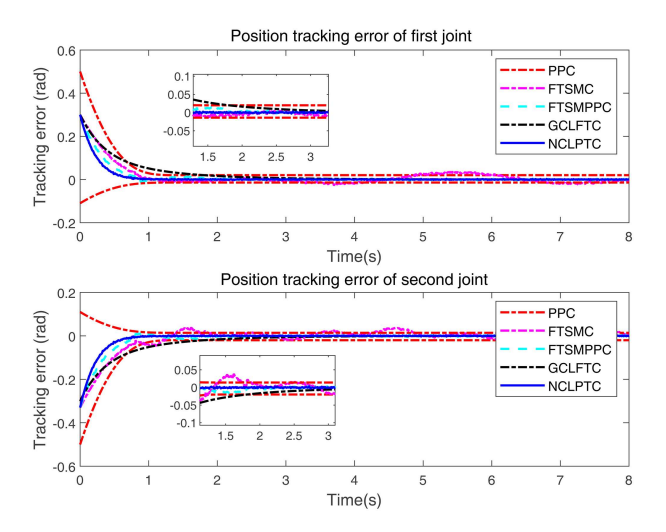
$$e_i \in (\underline{d}_i \chi_i, \bar{d}_i \chi_i).$$
 (48)

Additionally, Eq. (48) and Lemma 3 revealed that the position tracking, e_i , was always stable in $(\underline{d}_i\chi_i, \bar{d}_i\chi_i)$. Eq. (3) confirmed that e_i would be stable within $(\underline{d}_i\chi_{\infty i}, \bar{d}_i\chi_{\infty i})$ at T_i . Furthermore, Lemma 1 and Remark 2 confirmed that $\tilde{\theta}$ and e converged to zero within a predefined time, T_f , during which $T_f \leq T_s + T_c + T_e$, $T_s = \max\{T_{s1}, \ldots, T_{sn}\}$, and $T_c = \max\{T_{c1}, \ldots, T_{cn}\}$ are known positive constants. The proof is completed.

Remark 7. The PPF parameters can be selected based on actual needs. Parameters l_i and T_i determine the convergence rate of PPF. If the parameter, $\chi_{\infty i}$, is selected to approximately zero, the error, e_i , can be as small as desired. Thus, to achieve optimized performance, we can select a smaller $\chi_{\infty i}$. However, it must be noted that extremely small $\chi_{\infty i}$ will make the controller suffer from a peaking phenomenon. Other parameters are obtained through theoretical analysis, as well as by trial and error. To reduce chattering, we utilize the sat(·) function instead of the sign(·) function.

4 Experiment

For the experiment, we utilized the DENSO robotic arm (Type: VP-6242G; Figure 2). The DENSO VP-6242G robotic arm is a compact yet powerful industrial robot that is designed for versatility across various applications. It features a sleek design with a small footprint and reduced loading area, a maximum payload capacity of 2.5 kg, six movement axes for excellent maneuverability and precision, and a positioning repeatability of 0.02 mm, ensuring



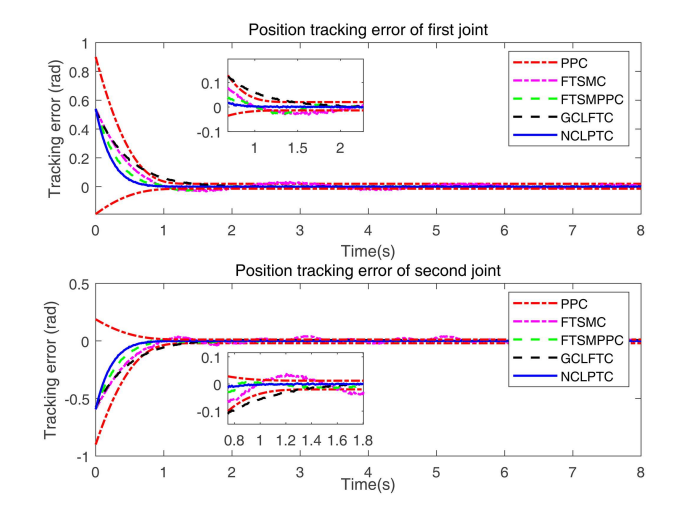


Figure 3 (Color online) Position-tracking errors under regulation trajectories with different controllers.

Figure 4 (Color online) Position-tracking errors under trajectories with different controllers.

high accuracy. Featuring energy-efficient motors rated below 80 W per axis and a total motor capacity of less than 300 W, VP-6242G supports applications such as material handling, palletizing, loading/unloading, and sealing. Its modular design ensures facile installation and maintenance, allowing for floor- and ceiling-mounted configurations, and its robust and reliable construction ensures consistent performance and longevity, making it an excellent choice for automated production lines across diverse industries. To ensure comprehensive comparisons, we conducted experiments for regulation and tracking scenarios.

Case 1. Regulation experiments were executed using a desired q_d , as follows:

$$\begin{bmatrix} \dot{q}_{di} \\ \ddot{q}_{di} \end{bmatrix} = \begin{bmatrix} 0 & 1 \\ -36 & -12 \end{bmatrix} \begin{bmatrix} q_{di} \\ \dot{q}_{di} \end{bmatrix} + \begin{bmatrix} 0 \\ 36 \end{bmatrix} q_{ci}, \tag{49}$$

where i=1,2. Our choice of (q_{c1},q_{c2}) followed that in [6]. The control gains and parameters were selected as $\mu_1=\mu_2=1.7, k_1=k_2=5, \Gamma=0.8I, \sigma=0.06, t_d=1.2 \text{ s}, T_e=0.3 \text{ s}, \hat{\theta}(0)=[0,0,0,0,0,0,0,0]^{\mathrm{T}}$. Let $\theta=[\theta_1,\theta_2,\theta_3,\theta_4,\theta_5,\theta_6,\theta_7]^{\mathrm{T}}$. The predefined-time was $T_{c1}=T_{c2}=0.8$, with $\eta=0.5$. The prescribed performance parameters were also selected, As follows: $\chi_{01}=0.5, \chi_{02}=0.1, \chi_{\infty 1}=\chi_{\infty 2}=0.02, t_1=t_2=1.5, \vartheta_1=\vartheta_2=0.2, T_1=T_2=0.9$. The fixed-time terminal sliding mode prescribed performance control (FTSMPPC) parameters in [37] were selected, as follows: $r=2.8, p=0.9, k=3, \sigma=3.2, \delta=0.02, K_0=[3\ 0;0\ 3], K_1=[0.003\ 0;0\ 0.003],$ and $K_2=[0.2\ 0;0\ 0.2]$. The fixed-time terminal sliding-mode control (FTSMC) parameters [39] were selected, as follows: $p=0.7, r=2.3, k=3, \delta=0.03, \sigma=2.5, K_a=[3\ 0;0\ 3], K_b=[2\ 0;0\ 4],$ and $K_c=[6\ 0,0\ 6]$.

The experimental results demonstrate that all the controllers perform well in trajectory tracking. Notably, the proposed NCLPTC exhibits a considerably faster convergence rate compared to FTSMPPC and FTSMC. Under FTSMC, the joint tracking error exhibits significant overshoot, and the tracking errors fail to remain within the predefined performance bounds (PPBs). Under FTSMPPC, although the tracking errors stay within the PPB. However, the convergence rate is notably slower than that of NCLPTC. The integration of the PPF in NCLPTC ensures that the tracking errors consistently stay within PPB. To further demonstrate the superior performance of the proposed NCLPTC, comparative experiments were conducted with the recently proposed GCLFTC in [19]. The comparative results are presented in Figures 3 and 4. As observed in Figures 3 and 4, the tracking error converges to zero significantly faster under the proposed NCLPTC scheme than with other methods, and the tracking error consistently remains within the PPB. The parameter convergence is shown in Figure 5. To facilitate a clear comparison of the parameter-identification condition, we display the scenarios of $\|\hat{\theta}\|$ in Figure 6(a). The estimation values obtained by (27) were realized more rapidly by the proposed control scheme than GCLFTC. Figure 7 shows the inputs of the different control schemes.

Case 2. The tracking experiments were conducted using a desired q_d generated through an inverse kinematics model [6]

$$\begin{cases} q_{d1} = \arctan\left(\frac{x_{d2}}{x_{d1}}\right) - \arctan\left(\frac{\sin(q_{d2})}{1 + \cos(q_{d2})}\right), \\ q_{d2} = \arctan(2x_{d1}^2 + 2x_{d2}^2 - 1). \end{cases}$$
(50)

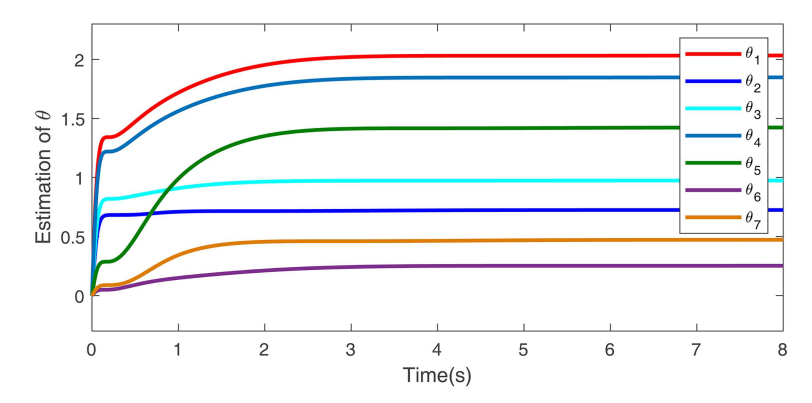


Figure 5 (Color online) Parameter-estimation under a regulation scenario.

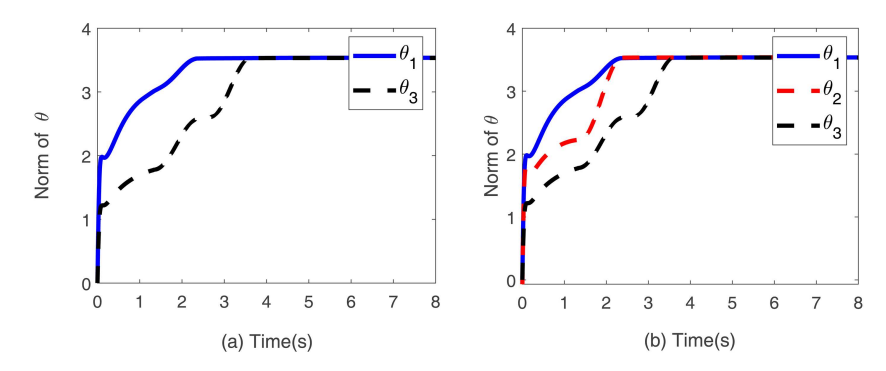


Figure 6 (Color online) Parameter-estimation performance. (a) represents the parameter identification condition in Case 1, and (b) represents the parameter-identification condition in Case 2.

The following control parameters were selected: $\mu_1 = \mu_2 = 1.3, k_1 = k_2 = 2, \Gamma = 0.6I, \sigma = 0.06, t_d = 1.2s, T_e = 0.5s, \hat{\theta}(0) = [0,0,0,0,0,0,0]^T$. The predefined-time was $T_{c1} = T_{c2} = 0.8$, with $\eta = 0.3$. The following prescribed performance parameters were selected: $\chi_{01} = 0.9, \chi_{02} = 0.2, \chi_{\infty 1} = \chi_{\infty 2} = 0.02, l_1 = l_2 = 1.7, \vartheta_1 = \vartheta_2 = 0.3, T_1 = T_2 = 0.9$. The FTSMPPC parameters in [37] were selected: $r = 2.4, k = 3, p = 0.7, \delta = 0.01, \sigma = 2.5, K_0 = [1\ 0,0\ 1], K_1 = [0.015\ 0,0\ 0.015], \text{ and } K_2 = [0.2\ 0,0\ 0.2)$. The FTSMC parameters in [39] were selected: $p = 0.7, r = 1.6, k = 3, \delta = 0.03, \sigma = 3.5, K_a = [1.5\ 0;0\ 1.5], K_b = [2.5\ 0;0\ 2.5], \text{ and } K_c = [1.5\ 0;0\ 1.5]$. The scenarios are illustrated in Figures 4, 8, 9, and 6(b). The scenarios exhibit a close resemblance to Case 1, achieving commendable outcomes regarding tracking-error minimization and parameter convergence.

Discussion. In the regulation and tracking scenarios, the results demonstrate that the proposed control scheme ensures that the parameter estimation and tracking errors converge to zero within a predefined time. This performance is primarily attributed to the incorporation of the prediction error in the CL law, which quantifies the discrepancy between the model's predicted values and the actual system observations. Compared with traditional adaptive methods, this approach enhances the speed and accuracy of parameter convergence while improving overall trajectory tracking performance. Due to the fact that the control force of a physical system cannot be infinitely large and inertia is inherent in the system, control switching is accompanied by hysteresis. Near the switching surface, the time lag in switching causes a delay in the precise change of state triggered by the control action. Furthermore, since the magnitude of the control variable gradually decreases with the magnitude of the state variable, this behavior appears as a decaying triangular wave superimposed on the smooth sliding-mode surface. Consequently, a "dead zone" for state-variable changes is formed in the state space, leading to control discontinuity and, consequently, the generation of chattering. The combined effect of these factors causes variable-structure control to exhibit high-frequency chattering in sliding mode. In this study, CL techniques are adopted to address unknown dynamics. Estimated values and regression matrices are incorporated into the controller to compensate for these unknown dynamics, thereby reducing reliance on switching terms. In addition, during experiments, the sign function is replaced with the hyperbolic tangent function to further suppress chattering. These approaches contribute to a smooth, continuous control process and effectively reduce chattering. In experiments, gains are typically adjusted to ensure that the system responds quickly and accurately to command changes. Appropriately increasing the gain can improve the system's response speed, enabling it to reach a new stable state rapidly. However, if the gain is set too high, it may lead to instability; if it is too low, the system may remain stable but respond sluggishly. In the

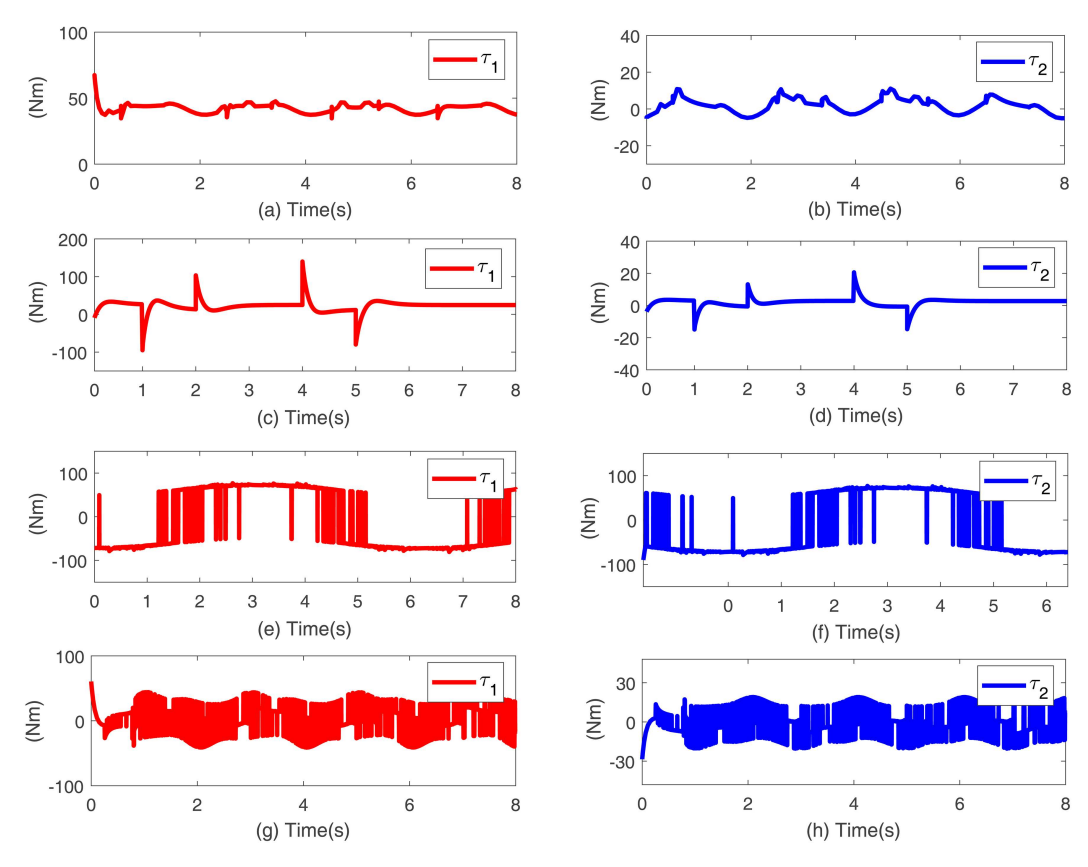


Figure 7 (Color online) Experimental requested inputs under regulation scenarios. (a), (c), (e), and (g) represent the Joint 1 control inputs of NCLPTC, GCLFTC, FTSMC, and FTSMPPC, respectively. (b), (d), (f), and (h) represent the Joint 2 control inputs of NCLPTC, GCLFTC, FTSMC, and FTSMPPC, respectively.

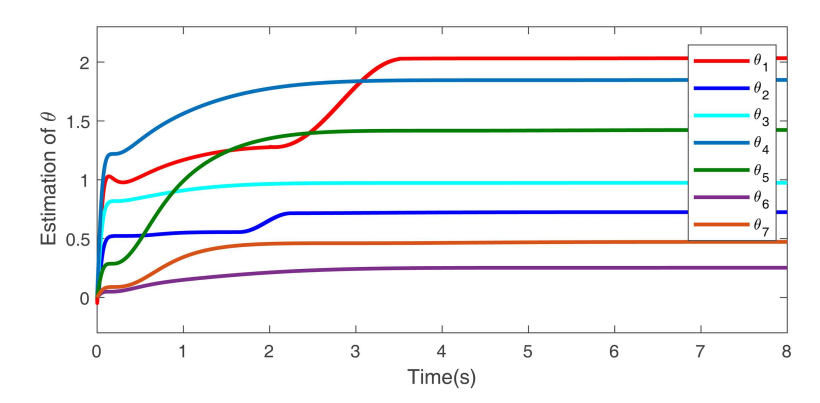


Figure 8 (Color online) Parameter estimation under a tracking scenario.

experimental process presented in this study, the initial gain was set to a small constant value. The parameters were then gradually increased based on the system's output response, ensuring that the selected gain produced effective control performance in practical applications.

5 Conclusion

In this paper, a novel nonsingular SMC method integrating variable-exponent coefficients with NCLPTC and PPC was presented for the PTC of robotic systems. By employing a simple variable-exponent coefficient in the sliding variable, the NCLPTC method achieved the prescribed performance without encountering singularities. Coupled with the predefined-time strategy, the concise relationship between the tuning gains and the predefined stabilization time was established. It demonstrated that the position-tracking error converged to and remained within the PPB

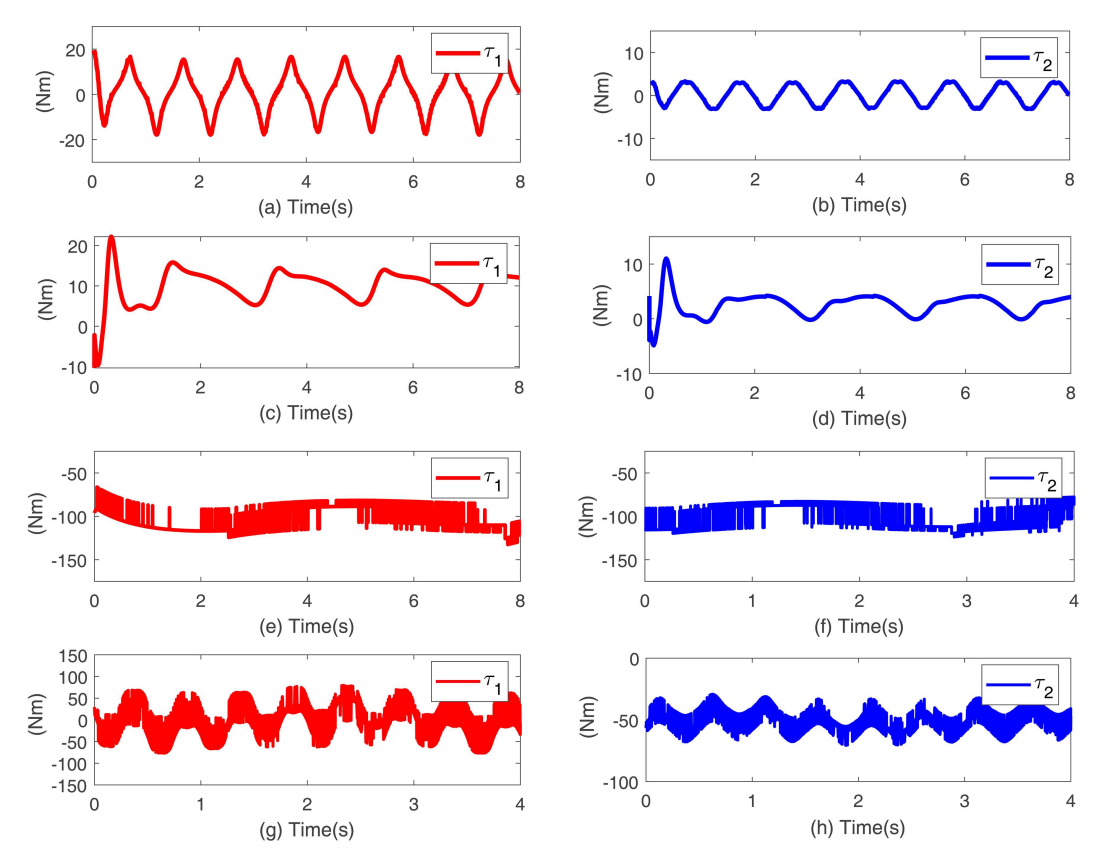


Figure 9 (Color online) Experimental requested inputs under the tracking scenario. (a), (c), (e), and (g) represent the Joint 1 control inputs of NCLPTC, GCLFTC, FTSMC, and FTSMPPC, respectively. (b), (d), (f), and (h) represent the Joint 2 control inputs of NCLPTC, GCLFTC, FTSMC, and FTSMPPC, respectively.

under a much weaker IE condition within a globally predefined time. The effectiveness and practical implementation of the proposed control schemes were experimentally demonstrated.

Acknowledgements This work was supported in part by S&T Program of Hebei (Grant Nos. 2024HBQZYCXY011, 242G1802Z), Natural Science Foundation of Hebei Province (Grant No. E2025210100), Science and Technology Project of Hebei Education Department (Grant Nos. QN2025159, BJ2025200), and National Natural Science Foundation of China (Grant Nos. 12202287, 12472020, 52405042). Both Yanshan University and Shijiazhuang Tiedao University are the first affiliations for this work.

References

- 1 Zhang F, Meng D Y, Cai K Q. Segment-wise learning control for trajectory tracking of robot manipulators under iteration-dependent periods. Sci China Inf Sci, 2024, 67: 132203
- 2 Luo Y, Ji T Y, Sun F C, et al. Robust tube-based MPC with smooth computation for dexterous robot manipulation. Sci China Inf Sci, 2024, 67: 212207
- 3 Zhang Y, Yang C G, Xu S, et al. Obstacle avoidance in human-robot cooperative transportation with force constraint. Sci China Inf Sci, 2023, 66: 119205
- 4 Altan A, Hacıöğlu R. Model predictive control of three-axis gimbal system mounted on UAV for real-time target tracking under external disturbances. Mech Syst Signal Process, 2020, 138: 106548
- 5 Altan A. Performance of metaheuristic optimization algorithms based on swarm intelligence in attitude and altitude control of unmanned aerial vehicle for path following. In: Proceedings of the 4th International Symposium on Multidisciplinary Studies and Innovative Technologies (ISMSIT), 2020. 1–6
- 6 Pan Y, Yu H. Composite learning robot control with guaranteed parameter convergence. Automatica, 2018, 89: 398–406
- 7 Ma X R, Li H Y, Liu J, et al. Adaptive coupled-sliding-variable-based finite-time control of composite formation for multi-robot systems. Sci China Inf Sci, 2024, 67: 202202
- 8 Ioannou P A, Sun J. Robust Adaptive Control. Upper Saddle River: PTR Prentice-Hall, 1996
- 9 Duarte M A, Narendra K S. Combined direct and indirect approach to adaptive control. IEEE Trans Automat Contr, 1989, 34: 1071–1075
- 10 Slotine J J E, Li W. Composite adaptive control of robot manipulators. Automatica, 1989, 25: 509–519
- 11 Narendra K S, Boskovic J D. A combined direct, indirect, and variable structure method for robust adaptive control. IEEE Trans Automat Contr, 1992, 37: 262–268
- 12 Guo K, Pan Y, Zheng D, et al. Composite learning control of robotic systems: a least squares modulated approach. Automatica, 2020, 111: 108612
- 13 Huang D, Yang C, Pan Y, et al. Composite learning enhanced neural control for robot manipulator with output error constraints. IEEE Trans Ind Inf, 2019, 17: 209–218
- 14 Sun T, Peng L, Cheng L, et al. Composite learning enhanced robot impedance control. IEEE Trans Neural Netw Learn Syst, 2019, 31: 1052-1059
- 15 Guo K, Pan Y, Yu H. Composite learning robot control with friction compensation: a neural network-based approach. IEEE Trans Ind Electron, 2018, 66: 7841–7851

- 16 Jiang Y, Wang Y, Miao Z, et al. Composite-learning-based adaptive neural control for dual-arm robots with relative motion. IEEE Trans Neural Netw Learn Syst, 2020, 33: 1010–1021
- 17 Guo K, Liu Y, Xu B, et al. Locally weighted learning robot control with improved parameter convergence. IEEE Trans Ind Electron, 2022, 69: 13236–13244
- 18 Zhang Y, Hua C. Composite learning finite-time control of robotic systems with output constraints. IEEE Trans Ind Electron, 2022, 70: 1687–1695
- 19 Zhang Y, Pang K, Hua C. Global composite learning fixed-time control of robotic systems with asymmetric tracking error constraints. IEEE Trans Ind Electron, 2022, 70: 7082–7091
- 20 Sánchez-Torres J D, Sanchez E N et al. Predefined-time stability of dynamical systems with sliding modes. In: Proceedings of the American Control Conference (ACC), 2015. 5842–846
- 21 Song Y, Wang Y, Holloway J, et al. Time-varying feedback for regulation of normal-form nonlinear systems in prescribed finite time. Automatica, 2017, 83: 243–251
- 22 Sánchez-Torres J D, Gómez-Gutiérrez D, López E, et al. A class of predefined-time stable dynamical systems. IMA J Math Control Inf, 2018, 35: i1-i29
- 23 Zhang M, Tong W, Li P, et al. Robust neural dynamics method for redundant robot manipulator control with physical constraints. IEEE Trans Ind Inf, 2023, 19: 11721–11729
- 24 Bechlioulis C P, Rovithakis G A. Adaptive control with guaranteed transient and steady state tracking error bounds for strict feedback systems. Automatica, 2009, 45: 532–538
- 25 Na J, Huang Y, Pei Q, et al. Active suspension control of full-car systems without function approximation. IEEE ASME Trans Mechatron, 2019, 25: 779–791
- 26 Hua C, Chen J, Li Y, et al. Adaptive prescribed performance control of half-car active suspension system with unknown dead-zone input. Mech Syst Signal Process, 2018, 111: 135–148
- 27 Hu Q, Shao X, Guo L. Adaptive fault-tolerant attitude tracking control of spacecraft with prescribed performance. IEEE ASME Trans Mechatron, 2017, 23: 331–341
- 28 Dai S L, He S, Chen X, et al. Adaptive leader-follower formation control of nonholonomic mobile robots with prescribed transient and steady-state performance. IEEE Trans Ind Inf, 2020, 16: 3662–3671
- 29 Haddad W M, Lee J. Finite-time stabilization and optimal feedback control for nonlinear discrete-time systems. IEEE Trans Automat Contr, 2023, 68: 1685–1691
- 30 Zhu C, Jiang Y, Yang C. Fixed-time neural control of robot manipulator with global stability and guaranteed transient performance. IEEE Trans Ind Electron, 2022, 70: 803–812
- 31 Wang L, Sun W, Su S F, et al. Adaptive asymptotic tracking control for flexible-joint robots with prescribed performance: design and experiments. IEEE Trans Syst Man Cybern Syst, 2023, 53: 3707–3717
- 32 Sharifi M, Azimi V, Mushahwar V K, et al. Impedance learning-based adaptive control for human-robot interaction. IEEE Trans Contr Syst Technol, 2022, 30: 1345–1358
- 33 Yu X, He W, Li H, et al. Adaptive fuzzy full-state and output-feedback control for uncertain robots with output constraint. IEEE Trans Syst Man Cybern Syst, 2021, 51: 6994–7007
- 34 Sun W, Su S F, Xia J, et al. Adaptive fuzzy tracking control of flexible-joint robots with full-state constraints. IEEE Trans Syst Man Cybern Syst, 2019, 49: 2201–2209
- 35 Munoz-Vazquez A J, Sánchez-Torres J D, Jimenez-Rodriguez E, et al. Predefined-time robust stabilization of robotic manipulators. IEEE ASME Trans Mechatron, 2019, 24: 1033–1040
- Zuo Z. Nonsingular fixed-time consensus tracking for second-order multi-agent networks. Automatica, 2015, 54: 305-309
- 37 Yang P, Su Y. Proximate fixed-time prescribed performance tracking control of uncertain robot manipulators. IEEE ASME Trans Mechatron, 2021, 27: 3275–3285
- 38 Farrell J A, Polycarpou M M. Adaptive Approximation based Control: Unifying Neural, Fuzzy and Traditional Adaptive Approximation Approaches. Hoboken: John Wiley & Sons, 2006
- 39 Su Y, Zheng C, Mercorelli P. Robust approximate fixed-time tracking control for uncertain robot manipulators. Mech Syst Signal Process, 2020, 135: 106379